

Cancelling microwave crosstalk with fixed-frequency qubits

Wuerkaixi Nuerbolati,¹ Zhikun Han,^{2,3,4} Ji Chu,^{2,3,4} Yuxuan Zhou,^{2,3,4}
Xinsheng Tan,^{1,*} Yang Yu,¹ Song Liu,^{2,3,4} and Fei Yan^{2,3,4,†}

¹National Laboratory of Solid State Microstructures, School of Physics, Nanjing University, Nanjing 210093, China

²Shenzhen Institute for Quantum Science and Engineering, Southern
University of Science and Technology, Shenzhen, Guangdong, China

³International Quantum Academy, Shenzhen, Guangdong, China

⁴Guangdong Provincial Key Laboratory of Quantum Science and Engineering,
Southern University of Science and Technology, Shenzhen, Guangdong, China

Scalable quantum information processing requires that modular gate operations can be executed in parallel. The presence of crosstalk decreases the individual addressability, causing erroneous results during simultaneous operations. For superconducting qubits which operate in the microwave regime, electromagnetic isolation is often limited due to design constraints, leading to signal crosstalk that can deteriorate the quality of simultaneous gate operations. Here, we propose and demonstrate a method based on AC Stark effect for calibrating the microwave signal crosstalk. The method is suitable for processors based on fixed-frequency qubits which are known for high coherence and simple control. The optimal compensation parameters can be reliably identified from a well-defined interference pattern. We implement the method on an array of 7 superconducting qubits, and show its effectiveness in removing the majority of crosstalk errors.

Crosstalk is a major factor that impedes the development of scalable quantum information processing architectures. Among the miscellaneous crosstalk phenomena including measurement crosstalk [1, 2], signal crosstalk [3–7] and quantum-mechanical crosstalk (spurious coupling) [8–11], the microwave signal crosstalk is notorious for superconducting qubits which usually operate at 4–8 GHz. Various technologies have been developed to improve isolation between circuit components to reduce such crosstalk [12–16]. As the integration level of quantum processors continue to increase, the presence of denser wires and more crowded spectrum unavoidably leads to adverse crosstalk effect. To remove microwave signal crosstalk, an effective approach is to offset the crosstalk signal with an out-of-phase compensation signal. This has been demonstrated in processors with tunable qubits where one is able to apply resonant driving and monitor the effectiveness of compensation [17]. However, the dynamic tuning range is limited due to design and fabrication variation, and the resonance condition may not be satisfied. Moreover, such a protocol is unsuitable for architectures based on fixed-frequency qubits which have recently been demonstrated with high-fidelity entangling operations using simple control [18–20].

In this work, we propose and demonstrate a method of microwave crosstalk calibration that is applicable to fixed-frequency qubits. Our protocol is based on the alternative-current (AC) Stark effect [21] or the Autler-Townes effect, by which a detuned crosstalk drive can induce a shift in the qubit frequency. Using a spin-echo sequence, we measure the Stark-induced phase, which shows a well-defined interference pattern with respect to the compensation drive parameters, which can be reliably optimized with increasing sequence duration. The qubit frequency measured using the Ramsey fringe is

found independent of the crosstalk signal amplitude, confirming the effectiveness in crosstalk compensation. Finally, we perform randomized benchmarking (RB) with simultaneous single-qubit gates on a chain of 7 fixed-frequency qubits. The result shows clear improvement from crosstalk compensation for all qubits, with up to 90% of signal crosstalk errors removed.

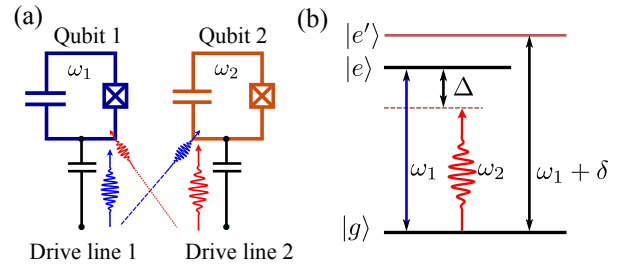


FIG. 1. (a) Schematic of microwave signal crosstalk. Two fixed-frequency transmon qubits have local drive lines sending microwave pulses at their respective frequency. Different colors indicate different frequencies. A smaller signal cross-talks to the other qubit. (b) The AC Stark effect in which the excited state ($|e\rangle$) of the target qubit is pushed higher to $|e'\rangle$ under a red-detuned crosstalk drive, resulting in a positive frequency shift δ .

We study the problem by first considering two fixed-frequency transmon qubits [22] where the nominally dedicated drive lines may couple to the other qubit, as illustrated in Fig. 1a. In general, the two qubits have different frequencies, ω_1 and ω_2 (assuming $\omega_1 > \omega_2$). Suppose that resonant pulses are applied to Qubit-2 for coherent operations. At the same time, Qubit-1 is also driven by these pulses due to crosstalk, though off-resonantly. According to the AC Stark effect, such off-resonant drive induces a

shift in the effective frequency of Qubit-1 by

$$\begin{aligned} \delta(\Omega, \Delta) &= \text{sgn}(\Delta)(\sqrt{\Omega^2 + \Delta^2} - |\Delta|) \\ &\approx \frac{\Omega^2}{2\Delta}, \end{aligned} \quad (1)$$

where $\Delta = \omega_1 - \omega_2$ is the detuning between the qubits and Ω is the equivalent Rabi frequency of the crosstalk drive. As displayed in the shown example (Fig. 1b), the Stark shift δ is positive when the drive is red-detuned ($\Delta > 0$), and negative the otherwise. The second line of Eq. (1) is the approximated form when $\Omega \ll |\Delta|$. Such a frequency shift is a main source of gate error because it changes the actual operating frequency of the qubit.

The crosstalk signal may be cancelled by interfering it with a compensation signal with the same shape, frequency and amplitude but 180° out-of-phase. However, because of the difference in overall attenuation and electromagnetic wave delay between drive line paths, the compensation signal has to be calibrated by using the qubit as the probe. In practice, because the wave delay between different drive lines (1 ns) is much shorter than the typical gate duration (30 ns), it is sufficient to calibrate the amplitude and phase only.

We first demonstrate our method in a two-qubit subsystem out of a 16-qubit processor, the design of which is similar to the device presented in Ref. [23]. The two transmon qubits have frequencies: 6.2497 GHz (target qubit) and 6.2718 GHz (control qubit).

They are separated in a qubit chain, and their coupling is negligible by design (~ 100 kHz). We apply to the target qubit the spin-echo sequence (Fig. 2a), which is known for its robustness against low-frequency noise and therefore provides better coherence time and signal visibility. Given a test pulse with certain amplitude A and phase ϕ applied to the control qubit drive line, crosstalk of this drive induces a Stark shift δ and hence a non-refocused phase on the target qubit during the echo sequence. Our goal is to search for the optimal compensation drive (phasor $\vec{r} = |r| \exp\{i\Delta\phi\}$) applied to the target qubit, which offsets the crosstalk drive (phasor \vec{r}^*). As shown in Fig. 2b, for a fixed τ , the measured response in the complex plane of the compensation phasor shows an interference pattern that resembles the Newton's rings. The center of the rings indicates the optimal working point for compensation; an additional 2π phase is accumulated for each ring outward. The pattern can be described by

$$S = \frac{1}{2} [1 + \cos(\delta(|\vec{r} + \vec{r}^*|A, \Delta) \cdot \tau)], \quad (2)$$

where S is the normalized signal.

Equation (2) implies that a longer free-evolution time τ reduces the oscillating period in the Newton's rings (faster ripples), effectively increasing the sensitivity to the Stark shift. Such an effect is illustrated in Fig. 2c

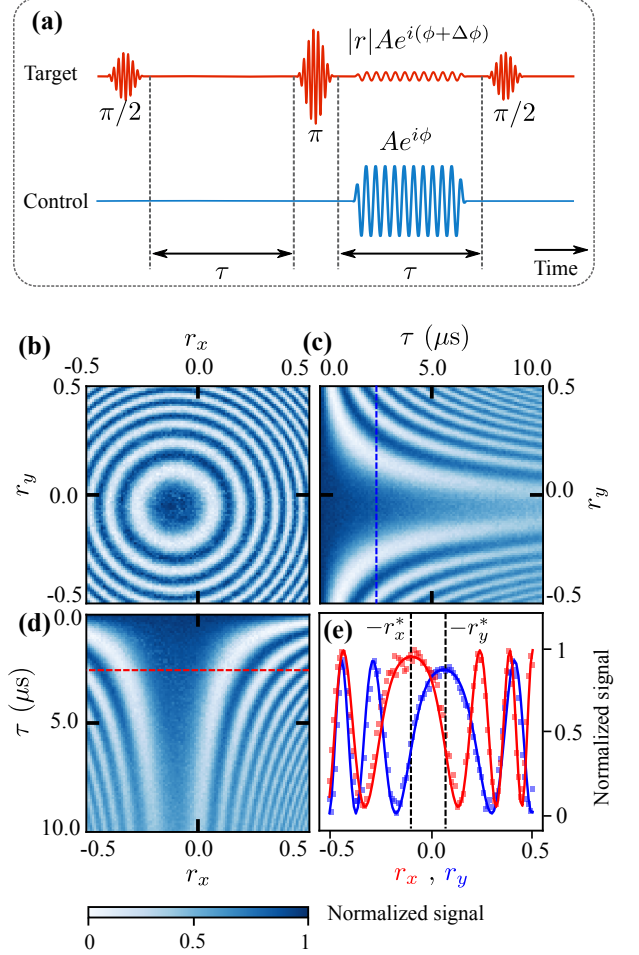


FIG. 2. (a) Pulse sequence for calibrating the crosstalk. A spin-echo pulse sequence (total free-evolution time: 2τ) is applied to the target qubit. A square-shaped resonant pulse with certain amplitude (A) and phase (ϕ) is applied to the control qubit during the second half of free-evolution period. The compensation pulse with relative amplitude ($|r|$) and phase ($\Delta\phi$) but at the control qubit frequency is simultaneously applied to the target qubit. (b) Measured response of the target qubit in the complex plane of the compensation phasor $\vec{r} = |r| \exp\{i\Delta\phi\}$, which resembles the Newton's rings. The center of the rings indicates where the crosstalk signal from the control qubit (phasor \vec{r}^*) is completely compensated, i.e., $\vec{r} + \vec{r}^* = 0$. (c,d) Target qubit response measured at $r_x = 0$ ((c)) and $r_y = 0$ ((d)) with varying free-evolution time τ , showing faster fringes with increased τ . (e) A linecut from (c) (blue) and (d) (red) measured at $\tau = 2.5 \mu\text{s}$, which are fitted to Eq. (2) for extracting the optimal compensation drive parameters $-\vec{r}^*$.

and Fig. 2d where we fix the real (r_x) and imaginary (r_y) part of the compensation phasor, respectively, but vary τ . Figure 2e shows a vertical ($r_x = 0$) and horizontal ($r_y = 0$) linecut measured at $\tau = 2.5 \mu\text{s}$, which are fitted to Eq. (2) for extracting the optimal compensation drive parameters. In practice, we progressively increase

τ during the parameter search to improve the accuracy, and we perform a gradient-based search algorithm during iterative measurements with a feedback loop to speed up the optimization process.

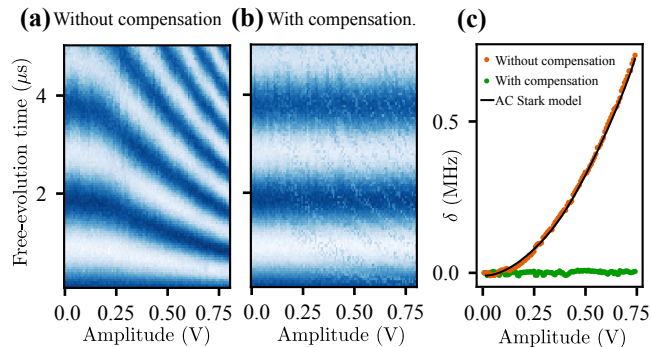


FIG. 3. Measured Ramsey fringes of the target qubit at different amplitude of the control drive (a) without and (b) with compensation. We intentionally add a baseline 500 kHz detuning for presentation purpose. (c) The extracted frequency shift in both cases showing the removal of the crosstalk effect across the whole amplitude range. The solid line is the fit to the Eq. (1).

Next, we verify our calibration by conducting a standard Ramsey experiment. The Ramsey fringe indicates the target-qubit frequency shift. We vary the amplitude of the test pulse applied to the control qubit and compare the measured Ramsey fringes without (Fig. 3a) and with (Fig. 3b) crosstalk compensation. Obviously, without compensation, the fringes become faster with increased drive amplitude, indicating stronger AC stark effect. With compensation, the fringes becomes stabilized and unaffected by the test pulse. We note that there exists small ripples, possibly as a result of imperfect compensation. The frequency shift δ in both cases are extracted and compared in Fig. 3c. Without compensation, the measured result is in good agreement with the AC stark effect as described in Eq. (1). The independence of the drive amplitude validates the linear response model of the crosstalk effect and assures the use of the optimization result to arbitrary waveforms.

Equation 2 indicates that the smallest detectable Stark shift depends on the sequence length τ . Therefore, the sensitivity of our method is proportional to the coherence time of the qubit. We may compare our method to the Rabi-based method. In the case of tunable qubits, the resonance condition $\Delta = 0$ is an extreme case in Eq. 1, where the Stark shift is maximized at $\delta = \Omega$. Experimentally, this may be done with a slow enough rise and fall for adiabatically ramping up the Stark shift. In this case, the Stark shift is equivalent to the Rabi method whose signal also oscillates at the Rabi frequency Ω . Both are limited by the coherence time. However, in the case of non-zero Δ such as for fixed-frequency qubits, the vis-

ibility of the Rabi oscillations are significantly reduced to $(\Omega/\Delta)^2$ in addition to decoherence, while the method based on Stark shift is unaffected.

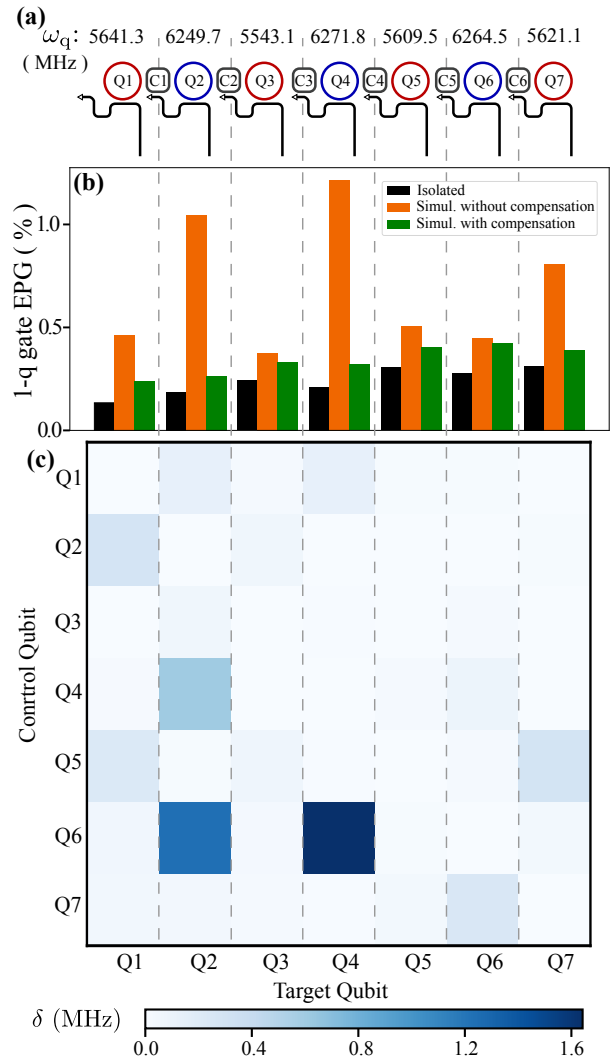


FIG. 4. (a) Schematic of an array of 7 fixed-frequency transmon qubits interleaved with tunable couplers. A shared control line is used to deliver both the microwave pulse to the qubit and the slow flux pulse to the coupler. (b) Error per gate (EPG) of single-qubit gates obtained by implementing RB separately (black), simultaneously without compensation (orange), and simultaneously with compensation (green). See Table. I for listed values. (c) The AC Stark shift matrix as an indicator of the crosstalk impact on the target qubit when driving the control qubit resonantly. For example, crosstalk from Q4 to Q6 shows the strongest shift due to their relatively small detuning ($\Delta = 5.5$ MHz), which is consistent with the error deterioration of Q4 in the simultaneous RB result.

To evaluate the performance of our method in the context of a more crowded system, we perform RB to an array of 7 qubits (Q1–Q7) on the same processor as depicted in Fig. 4a (Q2 and Q4 were used in the

RB error	Q1	Q2	Q3	Q4	Q5	Q6	Q7
■ (%)	0.13	0.19	0.24	0.21	0.31	0.28	0.31
■ (%)	0.46	1.05	0.37	1.21	0.50	0.45	0.81
■ (%)	0.24	0.26	0.33	0.32	0.41	0.42	0.39
■ (%)	67.5	90.9	32.2	89.2	49.6	14.4	84.2

TABLE I. Measured gate errors and the crosstalk error reduction ratio in each case corresponding to that in Fig. 4b.

previous demonstration). The qubit frequencies are interleaved between a lower-frequency (~ 5.6 GHz) and higher-frequency (~ 6.2 GHz) band. Since the neighboring qubits are largely detuned, even though their crosstalk amplitude is relatively stronger, the AC stark shift is still considerably smaller than that between qubits in the same frequency band. Therefore, we calibrate the crosstalk parameters for each pair of qubits in the same band only.

We performed simultaneous RB on all 7 qubits without compensation and compare the extracted error per gate (EPG) with that measured separately (orange versus black bars in Fig. 4b). All qubits show higher EPG as a result of crosstalk, for some qubits such as Q2 and Q4, the degradation is particularly significant, e.g., 6-fold EPG increase for Q4. The observation can be explained by the AC stark shift matrix (Fig. 4c) calculated from the measured crosstalk parameters and $\Omega = |r|\Omega_0$, where $\Omega_0 = 33$ MHz corresponding to the maximum Rabi frequency in a 30ns-long cosine-shaped pulse used in the experiment. From the matrix, we can easily identify that the AC stark effect induced by Q6 on Q2 and Q4 is much stronger because of the adjacency in their frequencies.

Finally, we performed the same simultaneous RB with crosstalk compensation turned on (green bars in Fig. 4b). All qubits show clear improvement compared to the case without compensation (green bars versus orange bars). In particular, most of the crosstalk error in Q1, Q2, Q4 and Q7 are removed, e.g., about 90% for Q2 and Q4, confirming the effectiveness of our method. The strongest crosstalk effect in these qubits – the maximum δ in each column of the matrix – comes from control qubits in the same frequency band where the compensation is implemented. Note that Q6 shows little improvement from compensation (only 14% crosstalk error reduction), even if the crosstalk effect from Q7 is still significant. This is because Q6 and Q7 are in different frequency bands and we did not implement inter-band compensation. In addition to the microwave crosstalk, the remaining errors (green bars versus black bars) may come from quantum-mechanical crosstalk effect such as the spectator effect [10, 11] as the change in the state of neighboring qubits can also cause a change in the frequency of the target qubit. In our device, there is on average a residual ZZ coupling strength of about 50 kHz. In addition, we note no performance degradation over time for the classical signal compensation, and the calibrated parameters are

unaffected between different cool-downs as long as the wiring is unchanged.

To summarize, we successfully implement a method based on the AC Stark effect to calibrate the microwave signal crosstalk ubiquitously seen in superconducting quantum processors. The method is an important addition to the calibration toolbox, especially suitable for qubits whose frequencies are non-tunable or subject to limited tunability.

We show that by crosstalk compensation we are able to remove the majority of crosstalk errors during simultaneous single-qubit gate operations. We also find that such microwave crosstalk phenomenon can be highly non-local, affecting far-neighbor qubits when their frequencies are close. In a frequency-crowded system, it is crucial to fully calibrate such crosstalk for global high performance of the quantum processors.

Acknowledgement: This work was supported by the Key-Area Research and Development Program of Guangdong Province (Grant No. 2018B030326001), the National Natural Science Foundation of China (U1801661), the Guangdong Innovative and Entrepreneurial Research Team Program (2016ZT06D348), the Guangdong Provincial Key Laboratory (Grant No.2019B121203002), the Natural Science Foundation of Guangdong Province (2017B030308003), the Science, Technology and Innovation Commission of Shenzhen Municipality (KYT-DPT20181011104202253), the Shenzhen-Hong Kong Cooperation Zone for Technology and Innovation (HZQB-KCZYB-2020050), and the NSF of Beijing (Grant No. Z190012). X.T. and Y.Y. acknowledge support from NSFC (Grant No. 61521001, No. 12074179 and No. 11890704) and NSF of Jiangsu Province (Grant No. 2021102024).

Data availability: The data that support the plots within this paper and other findings of this study are available from the corresponding authors upon reasonable request.

* tanxs@nju.edu.cn

† yanf7@sustech.edu.cn

- [1] F. Altomare, K. Cicak, M. A. Sillanpää, M. S. Allman, A. J. Sirois, D. Li, J. I. Park, J. A. Strong, J. D. Teufel, J. D. Whittaker, and R. W. Simmonds, Measurement crosstalk between two phase qubits coupled by a coplanar waveguide, *Physical Review B* **82**, 094510 (2010).
- [2] M. Khezri, J. Dressel, and A. N. Korotkov, Qubit measurement error from coupling with a detuned neighbor in circuit QED, *Physical Review A* **92**, 052306 (2015).
- [3] J. Wenner, M. Neeley, R. C. Bialczak, M. Lenander, E. Lucero, A. D. O’Connell, D. Sank, H. Wang, M. Weides, A. N. Cleland, and J. M. Martinis, Wirebond crosstalk and cavity modes in large chip mounts for superconducting qubits, *Superconductor Science and Technology* **24**, 065001 (2011).

- [4] X. Dai, D. Tennant, R. Trappen, A. Martinez, D. Melanson, M. Yurtalan, Y. Tang, S. Novikov, J. Grover, S. Disseler, J. Basham, R. Das, D. Kim, A. Melville, B. Niedzielski, S. Weber, J. Yoder, D. Lidar, and A. Lupascu, Calibration of Flux Crosstalk in Large-Scale Flux-Tunable Superconducting Quantum Circuits, *PRX Quantum* **2**, 040313 (2021).
- [5] D. M. Abrams, N. Didier, S. A. Caldwell, B. R. Johnson, and C. A. Ryan, Methods for Measuring Magnetic Flux Crosstalk Between Tunable Transmons, *Physical Review Applied* **12**, 064022 (2019).
- [6] S. Huang, B. Lienhard, G. Calusine, A. Vepsäläinen, J. Braumüller, D. K. Kim, A. J. Melville, B. M. Niedzielski, J. L. Yoder, B. Kannan, T. P. Orlando, S. Gustavsson, and W. D. Oliver, Microwave Package Design for Superconducting Quantum Processors, *PRX Quantum* **2**, 020306 (2021).
- [7] P. A. Spring, S. Cao, T. Tsunoda, G. Campanaro, S. D. Fasciati, J. Wills, V. Chidambaram, B. Shteynas, M. Bakr, P. Gow, *et al.*, High coherence in a tileable 3d integrated superconducting circuit architecture, *arXiv preprint arXiv:2107.11140* (2021).
- [8] P. Mundada, G. Zhang, T. Hazard, and A. Houck, Suppression of Qubit Crosstalk in a Tunable Coupling Superconducting Circuit, *Physical Review Applied* **12**, 054023 (2019).
- [9] A. Patterson, J. Rahamim, T. Tsunoda, P. Spring, S. Jebari, K. Ratter, M. Mergenthaler, G. Tancredi, B. Vlastakis, M. Esposito, and P. Leek, Calibration of a Cross-Resonance Two-Qubit Gate Between Directly Coupled Transmons, *Physical Review Applied* **12**, 064013 (2019).
- [10] P. Zhao, K. Linghu, Z. Li, P. Xu, R. Wang, G. Xue, Y. Jin, and H. Yu, Quantum crosstalk analysis for simultaneous gate operations on superconducting qubits, *arXiv:2110.12570 [quant-ph]* (2021).
- [11] T.-Q. Cai, X.-Y. Han, Y.-K. Wu, Y.-L. Ma, J.-H. Wang, Z.-L. Wang, H.-Y. Zhang, H.-Y. Wang, Y.-P. Song, and L.-M. Duan, Impact of Spectators on a Two-Qubit Gate in a Tunable Coupling Superconducting Circuit, *Physical Review Letters* **127**, 060505 (2021).
- [12] Z. Chen, A. Megrant, J. Kelly, R. Barends, J. Bochmann, Y. Chen, B. Chiaro, A. Dunsworth, E. Jeffrey, J. Y. Mutus, P. J. J. O'Malley, C. Neill, P. Roushan, D. Sank, A. Vainsencher, J. Wenner, T. C. White, A. N. Cleland, and J. M. Martinis, Fabrication and characterization of aluminum airbridges for superconducting microwave circuits, *Applied Physics Letters* **104**, 052602 (2014).
- [13] A. Dunsworth, R. Barends, Y. Chen, Z. Chen, B. Chiaro, A. Fowler, B. Foxen, E. Jeffrey, J. Kelly, P. V. Klimov, E. Lucero, J. Y. Mutus, M. Neeley, C. Neill, C. Quintana, P. Roushan, D. Sank, A. Vainsencher, J. Wenner, T. C. White, H. Neven, J. M. Martinis, and A. Megrant, A method for building low loss multi-layer wiring for superconducting microwave devices, *Applied Physics Letters* **112**, 063502 (2018).
- [14] D. Rosenberg, S. J. Weber, D. Conway, D.-R. W. Yost, J. Mallek, G. Calusine, R. Das, D. Kim, M. E. Schwartz, W. Woods, J. L. Yoder, and W. D. Oliver, Solid-State Qubits: 3D Integration and Packaging, *IEEE Microwave Magazine* **21**, 72 (2020).
- [15] K. Wei, E. Magesan, I. Lauer, S. Srinivasan, D. Bogorin, S. Carnevale, G. Keefe, Y. Kim, D. Klaus, W. Landers, *et al.*, Quantum crosstalk cancellation for fast entangling gates and improved multi-qubit performance, *arXiv preprint arXiv:2106.00675* (2021).
- [16] B. K. Mitchell, R. K. Naik, A. Morvan, A. Hashim, J. M. Kreikebaum, B. Marinelli, W. Lavrijsen, K. Nowrouzi, D. I. Santiago, and I. Siddiqi, Hardware-efficient microwave-activated tunable coupling between superconducting qubits, *Physical review letters* **127**, 200502 (2021).
- [17] Y. Sung, L. Ding, J. Braumüller, A. Vepsäläinen, B. Kannan, M. Kjaergaard, A. Greene, G. O. Samach, C. McNally, D. Kim, A. Melville, B. M. Niedzielski, M. E. Schwartz, J. L. Yoder, T. P. Orlando, S. Gustavsson, and W. D. Oliver, Realization of high-fidelity CZ and ZZ-free iSWAP gates with a tunable coupler, *arXiv:2011.01261 [quant-ph]* (2020).
- [18] M. C. Collodo, J. Herrmann, N. Lacroix, C. K. Andersen, A. Remm, S. Lazar, J.-C. Besse, T. Walter, A. Wallraff, and C. Eichler, Implementation of Conditional Phase Gates Based on Tunable Z Z Interactions, *Physical Review Letters* **125**, 240502 (2020).
- [19] Y. Xu, J. Chu, J. Yuan, J. Qiu, Y. Zhou, L. Zhang, X. Tan, Y. Yu, S. Liu, J. Li, F. Yan, and D. Yu, High-Fidelity, High-Scalability Two-Qubit Gate Scheme for Superconducting Qubits, *Physical Review Letters* **125**, 240503 (2020).
- [20] J. Stehlik, D. M. Zajac, D. L. Underwood, T. Phung, J. Blair, S. Carnevale, D. Klaus, G. A. Keefe, A. Carniol, M. Kumph, M. Steffen, and O. E. Dial, Tunable Coupling Architecture for Fixed-Frequency Transmon Superconducting Qubits, *Physical Review Letters* **127**, 080505 (2021).
- [21] D. I. Schuster, A. Wallraff, A. Blais, L. Frunzio, R.-S. Huang, J. Majer, S. M. Girvin, and R. J. Schoelkopf, ac stark shift and dephasing of a superconducting qubit strongly coupled to a cavity field, *Phys. Rev. Lett.* **94**, 123602 (2005).
- [22] J. Koch, T. M. Yu, J. Gambetta, A. A. Houck, D. I. Schuster, J. Majer, A. Blais, M. H. Devoret, S. M. Girvin, and R. J. Schoelkopf, Charge-insensitive qubit design derived from the Cooper pair box, *Physical Review A* **76**, 042319 (2007).
- [23] J. Chu, X. He, Y. Zhou, J. Yuan, L. Zhang, Q. Guo, Y. Hai, Z. Han, C.-K. Hu, W. Huang, H. Jia, D. Jiao, Y. Liu, Z. Ni, X. Pan, J. Qiu, W. Wei, Z. Yang, J. Zhang, Z. Zhang, W. Zou, Y. Chen, X. Deng, X. Deng, L. Hu, J. Li, D. Tan, Y. Xu, T. Yan, X. Sun, F. Yan, and D. Yu, Scalable algorithm simplification using quantum AND logic, *arXiv:2112.14922 [quant-ph]* (2021).